Comparison of several models for the determination of the phase transformation yield surface in shape-memory alloys with experimental data

Christian Lexcellent*, Anja Schlömerkemper†

September 8, 2006

Keywords: shape-memory alloys (SMA), polycrystals, martensitic phase transformation, mechanical properties (elastic behavior, yield phenomena), theory.

Abstract

Proportional biaxial loadings (tension(compression)-internal pressure, bicompression) permit the experimental determination of the phase transformation yield surface in the stress space (e.g., the appearance of the martensitic phase inside the austenitic one). We review several theoretical, phenomenological and mathematical models which calculate the phase transformation yield surface obtained with multiaxial proportional loading experiments. Furthermore we compare the predictions with experiments.

1 Introduction

Shape-memory alloys show, among other effects, the so-called pseudo-elastic behavior. This behavior occurs at constant external temperature above the austenite finish temperature. At this temperature, the shape-memory alloy is in its austenitic state. It transforms to martensite upon a sufficiently strong applied load. The smallest stress at which this happens is called phase transformation initiation yield stress, phase transformation yield stress or yield stress for short, in analogy to the notion in plasticity theory. We refer to [1] and [2] for an introduction to the basic concepts of shape-memory alloys.

There is quite a number of experimental and theoretical works in which the pseudo-elastic behavior of shape-memory alloys is studied. In particular, there are experiments reported

*Laboratoire de Mécanique Appliquée R. Chaléat, FEMTO-ST. Université de Franche Comté, 24, chemin de l'Epitaphe, 25000 Besançon, France, christian.lexcellent@univ-fcomte.fr

†Corresponding author. Max-Planck-Institute for Mathematics in the Sciences, Inselstraße 22–26, D-04103 Leipzig, Germany, Tel.: +49-341-9959-547, Fax: +49-341-9959-633, schloem@mis.mpg.de

which show a different behavior in tension and compression, see e.g., [3, 4, 5, 6]. Related one-dimensional models as for instance the one developed by Šittner and coworkers [7, 8] deliver precious information to the physical meaning of the phase transformation; see also [9, 10].
In this article, however, we focus on the pseudo-elastic behavior of shape-memory alloys in loading experiments in more than one space dimension. That is, we consider experimental radial loading in the stress space and related models in more than one space dimension. These experiments and models determine yield surfaces or yield curves in the stress space rather than only the values for the yield stress in pure tension and compression. Inside the yield curve, the shape-memory alloy is in its austenitic phase. If the stress is on the yield curve, the material begins to transform, and if the stress is outside of this curve, the alloy is in a two phase state of austenite and martensite.

The outline of this article is as follows. In Section 2 we recall a few experimental results briefly and focus on the experiments performed by Bouvet et al. [11], which are interesting as they are based on multiaxial loading. An extrapolation of the experimental data gives the yield-curve, which shows an asymmetry in tension and compression and a mirror symmetry about the $\sigma_1 = \sigma_2$-axis, see below.
In Sections 3 to 6 we review three-dimensional models of polycrystalline shape-memory alloys which determine transformation yield surfaces under multiaxial loading. As we point out below, all these models have different assumptions and apply different methods. Still, they essentially recover the experimentally observed yield surfaces.
We start with a phenomenological model at the macroscopic scale (Section 3). Then we consider two models which use some micro-macro scheme; one (Section 4) is a so-called self-consistent model in the framework of thermodynamics, the other (Section 5) is based on a numerical simulation and the crystallographic theory of martensite initiated by Ball and James [12, 13]. In Section 6 we come to a model in the framework of energy minimization, which is also based on the crystallographic theory of martensite and which applies ideas of work by Bhattacharya and Kohn [14] in homogenization.

In Section 7 we compare the presented models among each other and with the experiments. This discussion results in a formulation of several open problems for future experimental, theoretical and mathematical works. In the appendix we summarize the notations used in this article.

2 Experimental results

In this section we mention briefly some experiments in order to present the main observations, which are interesting with respect to the models discussed below.
At the yield surface, the alloy transforms from austenite to martensite. Hence one needs measurement techniques which allow the determination of martensite inside the sample. Sometimes this is done approximately by studying the surface of the sample with optical instruments. The martensite volume fraction inside the sample can be determined by resistivity measurements. Such experiments were performed in tension and compression tests

with "in situ" resistivity measurements on CuZnAl polycrystals, cf. [6].
There are several experimental methods available to perform multiaxial loading experiments: Experimental results in pure tensile and compressive shear loadings on NiTi polycrystals are reported by Orgéas and Favier [4]. Raniecki et al. [5] determine the yield surface under tension(compression)-torsion on NiTi tubes, see also [15]. Gall et al. [16] performed triaxial proportional loading on CuZnAl cylinder specimens, where the pressure on the circumference surface is different from the one applied to the bottom and the top of the cylinder.
The above experiments were all performed on polycrystalline samples. Vivet and Lexcellent [17] determine the yield surface for a CuZnAl single crystal under bitraction. Figure 1 shows their experimental and numerical results.
Last but not least, Bouvet et al. [11] performed multiaxial proportional loading experiments on CuAlBe shape-memory alloys. In order to obtain data for at least three quadrants of the two dimensional eigenstress plane, they studied tension(compression)-internal pressure experiments on tubular specimens as well as bicompression experiments on cubic specimens. See Figure 2 for their results. The extrapolated yield curve shows an asymmetry in tension and compression. Moreover, the curve has a mirror symmetry with respect to the $\sigma_1 = \sigma_2$-axis. Similar tests were done on CuZnAl [18].
Finally, we mention that the dependence on temperature was studied [5, 11], cf. Section 3.

3 Phenomenological model at the macroscopic scale

The context of the phenomenological model reviewed in this section is thermodynamics. In the physical context of shape-memory alloys and other metallic alloys, thermodynamic potentials are in general written as Gibbs functions $G(\boldsymbol{\sigma}, T, z)$ or free energy Helmholtz functions $\phi(\boldsymbol{\varepsilon}, T, z)$, where $\boldsymbol{\sigma}$ and $\boldsymbol{\varepsilon}$ are the stress and strain tensors, respectively; T is the temperature and z some internal variable. Here, z denotes the volume fraction of martensite inside the austenite. The thermodynamic force associated to the advance of the phase transformation is given by

$$\Pi^f = -\frac{\partial G}{\partial z}. \tag{1}$$

In this context, the Clausius-Duhem inequality (or second law of thermodynamics) reads

$$\delta D = \Pi^f \, dz \geq 0,$$

where δD denotes the increment of dissipation D (and δ indicates that δD is not an exact differential). In the forward phase transformation, where austenite A transforms to martensite M, we have $dz > 0$ and thus $\Pi^f \geq 0$; in the reverse phase transformation $M \to A$, the Clausius-Duhem inequality yields $\Pi^f \leq 0$. The phase transformation begins when Π^f vanishes or attains a constant value in agreement with the Clausius-Duhem inequality condition. The choices of an explicit thermodynamic potential and of two yield functions for phase transformation: one for the forward transformation $A \to M$, $\Psi^{AM}(\boldsymbol{\sigma}, T, z)$ and another, $\Psi^{MA}(\boldsymbol{\sigma}, T, z)$, for the reverse transformation delivers the modeling of pseudoelasticity

in shape memory alloys. For instance, Ψ^{AM}, Ψ^{MA} are chosen as

$$\begin{aligned}\Psi^{AM}(\boldsymbol{\sigma}, T, z) &= \Pi^f(\boldsymbol{\sigma}, T, z) - \Pi^{AM}_{cr}(T, z)\\ \Psi^{MA}(\boldsymbol{\sigma}, T, z) &= -\Pi^f(\boldsymbol{\sigma}, T, z) + \Pi^{MA}_{cr}(T, z)\end{aligned}$$

under the conditions $\dot{\Psi}^{AM} = 0$ for $A \to M$ and $\dot{\Psi}^{MA} = 0$ for $M \to A$. Under these conditions, the yield function for the phase transformation initiation ($A \to M$), which is assumed to be convex in the stress space) can be written as

$$\Psi^{AM}(\boldsymbol{\sigma} = \boldsymbol{\sigma}^{AM}, T, z = 0) = \Pi^f(\boldsymbol{\sigma} = \boldsymbol{\sigma}^{AM}, T, z = 0) - \Pi^{AM}_{cr}(T) = 0.$$

The model that we review here is a phenomenological model that was derived by Bouvet et al. [19] in connection with their experimental results described in [11], cf. Section 2. This model is called J_2-J_3 criterion in reference to the second invariant $-J_2$ and the third invariant J_3 of the deviatoric stress tensor, see below. Note that $J_2 > 0$ by this definition.
The idea behind this model is the following: for forward transformation (austenite to martensite), the yield surface plays the same rôle as the yield surface in elasto-plastic transformations. The phenomenological model is developed in this spirit. It is assumed that the shape-memory alloy is isotropic, i.e., all grains are randomly oriented such that no direction is preferred. Moreover, it is assumed that the austenite-martensite transformation is volume-invariant, which means that the transformation yield surface does not depend on the first stress invariant $\frac{1}{3}\,\mathrm{Trace}(\boldsymbol{\sigma})$. Hence the yield stress is assumed to depend on the second, $-J_2$, and third, J_3, invariants of the deviatoric part of the stress tensor $\boldsymbol{\sigma}$; the deviatoric part of $\boldsymbol{\sigma}$ is given by $\mathrm{dev}\,\boldsymbol{\sigma} = \boldsymbol{\sigma} - \frac{1}{3}\,\mathrm{Trace}(\boldsymbol{\sigma})$. We express J_2 in terms of $\bar{\sigma}$, the Huber-Von Mises invariant,

$$\bar{\sigma} = \sqrt{3J_2} = \sqrt{\frac{3}{2}\,\mathrm{dev}\,\boldsymbol{\sigma} : \mathrm{dev}\,\boldsymbol{\sigma}},$$

where $\mathbf{A} : \mathbf{B} = \mathrm{Trace}(\mathbf{A}^T\mathbf{B})$ denotes the inner product of two matrices $\mathbf{A}$ and $\mathbf{B}$, and $\mathbf{A}^T$ is the transposed matrix of $\mathbf{A}$. The third deviatoric stress tensor invariant J_3 is $\det(\mathrm{dev}\,\boldsymbol{\sigma})$.
Bouvet et al. [11, 19] then introduce a nondimensional quantity

$$y = y(J_2, J_3) = \frac{27}{2}\frac{\det(\mathrm{dev}\,\boldsymbol{\sigma})}{\bar{\sigma}^3}.$$

Note that $y \in [-1, 1]$, where $y = 1$ corresponds to pure tension. Similarly, $y = -1$ is related to pure compression and $y = 0$ represents pure shear.
Bouvet et al. [11, 19] define also a function f and a so-called equivalent stress $\sigma_{\mathrm{eq}} = \bar{\sigma}g(y)$ such that the transformation yield surface is described by

$$f(\bar{\sigma}, y, \sigma_0) = \sigma_{\mathrm{eq}} - \sigma_0(T) = \bar{\sigma}g(y) - \sigma_0(T) = 0$$

with $\sigma_0(T) = b(T - M^0_S)$, where M^0_S is the martensite start temperature in the stress free state and $b > 0$ is a material constant. The function g is chosen in such a way that it fits the experimental points.

In experiments, $\sigma_0(T)$ equals the yield stress in pure tension along the eigenstress coordinate. In [11, 19], g is chosen as

$$g(y) = \cos\Big(\frac{\arccos(1 - a(1 - y))}{3}\Big),$$

where a is some material parameter. This gives a convex yield surface for all $a \in [0, 1]$. For CuAlBe polycrystals, the parameter a is chosen to be 0.7, which leads to the thick line in Figure 3 below, which agrees well with the experimental points. Similar results were obtained in CuZnAl polycrystals in [18].

As another example for a choice of the function g, we quote Raniecki et al. [5], who consider a NiTi alloy. They postulate the following empirical formula for $g(y)$ such that $g(y = 0) = 1$, where $y = 0$ corresponds to pure shearing:

$$g(y) = h - c\exp(-d(y + 1))$$

with $h = 1.17$, $c = 0.37$ and $d = 0.78$ for the NiTi alloy investigated. This gives the yield curves in Figure 4, which show the asymmetry in tension and compression as well as the effect of temperature.

The agreement of the phenomenological model with the experimental data is good for the two choices of $g(y)$ above.

4 Self-consistent scheme for 'micro-macro' integration

In this section we present another phenomenological model, developed by the team of Patoor, cf. [20, 21] and [22]. It studies a dependence on texture and is based on a so-called micro-macro scheme and uses a Gibbs free energy G, which is related to martensite transformations in single grains. The form of the Gibbs free energy used was established by Siredey et al. [23] in order to derive constitutive equations for polycrystalline thermoelastic shape-memory alloys.

Let n denote the number of habit plane variants and let $\boldsymbol{\epsilon}_i^t$ be the transformation strain tensor corresponding to the ith habit plane. The phase transformation strain $\boldsymbol{\epsilon}_i^t$ is calculated within the phenomenological theory by Wechsler et al. [24] developed in 1953:

$$\boldsymbol{\epsilon}_i^t = \frac{1}{2}(\mathbf{b}_i \otimes \mathbf{m}_i + \mathbf{m}_i \otimes \mathbf{b}_i),$$

where $\mathbf{m}_i$ and $\mathbf{b}_i$ are the habit plane normal and the shape strain vector corresponding to the habit plane variant i.

Let $\boldsymbol{\sigma}$ and T denote as before the external stress and the temperature, respectively. Moreover, let z_i be the volume fraction of the ith habit plane variant inside the grain considered. Then the Gibbs free energy in the self-consistent scheme reads [23]

$$G(\boldsymbol{\sigma}, T, z_1, \ldots, z_n) = \frac{1}{2}\boldsymbol{\sigma} : \mathbf{S}\,\boldsymbol{\sigma} + \boldsymbol{\sigma} : \sum_{i=1}^{n} \boldsymbol{\epsilon}_i^t z_i - B(T - T_0)\sum_{i=1}^{n} z_i - \frac{1}{2}\sum_{\substack{i,j=1 \\ i\neq j}}^{n} H^{ij} z_i z_j,$$

where $\mathbf{S}$ is the stiffness matrix and H^{ij} denotes an interaction matrix between martensite habit plane variants which only depends on known transformation strains.

The physical constraints $z_i \geq 0$ for each and $\sum_{i=1}^{n} z_i \leq 1$ for the whole volume fraction of martensite are taken into account in the model of Siredey et al. [23]. They compute the thermodynamic force $\Pi_i^f = -\frac{\partial G}{\partial z_i}$ for each volume fraction z_i, cf. (1), and they assume that the phase transformation starts when Π_i^f attains a critical value Π_i^{cr}.

Next, we come to the results obtained by Aleong et al. [20], Arbab Chirani and Patoor [21], and Arbab Chirani et al. [22] based on this model. In the numerical simulations in these works, polycrystalline materials are represented by N grains with N chosen to be 1000. The self-consistent method offers a straightforward solution of the global problem. This is done by summing the effects of each individual grain. For this, each grain is considered as being embedded within an effective medium which has average properties of the ensemble of grains. Moreover, the grains are assumed to be spherical for simplicity. By this method, one problem with N inclusions is transformed into N problems with one inclusion each. By doing this, any interaction of neighboring grains is neglected.

Moreover, different initial textures are implemented. The influence of the initial texture on the surfaces of constant total strain $\bar{\boldsymbol{\epsilon}}$ in CuZnAl is shown in Figure 5 [20], which is interesting also with respect to the model in Section 6. The curves show the expected asymmetry in tension and compression. Moreover, the plot for an isotropic crystal shows a symmetry with respect to the $\sigma_1 = \sigma_2$-axis, which does not precisely hold for the material with rolled texture. Nowadays, experiments are in progress to determine the yield points associated to some rolled and drawn CuAlBe samples in order to study the influence of texture on the yield surface experimentally [25].

To sum up, the self-consistent method is valid for any type of loading condition (proportional or non proportional). The parameters which are put into the simulations are crystallographic parameters ($\boldsymbol{\epsilon}_i^t$, $i = 1, \ldots, n$ with $n = 24$ for CuZnAl, for instance), thermodynamic parameters (T_0, B) and the coefficients of the interaction matrix H^{ij}, which are chosen phenomenologically.

Finally, we remark that there is a self-consistent model by Entemeyer et al. [26] in which an intergranular stress field is taken into account. This stress field models transformation strain incompatibilities from grain to grain. Entemeyer et al. use a homogenization procedure to determine the overall behavior.

5 'Micro-macro' integration based on the crystallographic theory of martensite

The crystallographic theory of martensite CTM, which is applied in this section, is different from the phenomenological crystallographic theory of Wechsler, Liebermann and Read [24], called WLR and used in Section 4. The CTM following Ball and James [12, 13] derives the microstructure from an energy minimization and does not require an "a priori" knowledge

of twinning modes (as is the case in the WLR theory). See [1] for an introduction to this topic. Next we recall basic concepts of the CTM, before we discuss a model by Lexcellent et al. [18] for the determination of the yield surface.

In this theory, the austenite is considered as the reference configuration; and the martensite is considered as a deformed configuration. Accordingly, the martensite is described by a deformation gradient $\mathbf{F}$; and the undistorted austenite is described by the identity matrix $\mathbf{1}$. At interfaces between martensite ($\mathbf{F}$) and undistorted austenite ($\mathbf{1}$), the compatibility condition

$$\mathbf{F} - \mathbf{1} = \mathbf{b} \otimes \mathbf{m} \tag{2}$$

must hold, where $\mathbf{m}$ is the unit normal at the interface and $\mathbf{b}$ is some vector in $\mathbb{R}^3$, called shape strain vector. The matrix $\mathbf{F}$ (with $\det \mathbf{F} > 0$) can uniquely be decomposed as follows: $\mathbf{F} = \mathbf{QU}$ with $\mathbf{U} = \sqrt{\mathbf{F}^T\mathbf{F}}$ and $\mathbf{Q}$ a rotation matrix. The different variants of martensite can now be described by the matrices $\mathbf{U}_i$, $i = 1, \ldots, \nu$, where ν is the number of martensite variants. Following the CTM, an exact interface between austenite and a single variant of martensite exists if and only if $\mathbf{U}_i$ has eigenvalues $\lambda_1, \lambda_2, \lambda_3$ such that $\lambda_1 \leq \lambda_2 = 1 \leq \lambda_3$. This condition is fulfilled for some Copper based alloys, e.g., CuAlBe and CuZnAl, see below and cf. [27]. It is not satisfied for CuAlNi and for NiTi based alloys, see, e.g., [28, Table 1] or [29].

Next we discuss the case $\lambda_2 = 1$ in the context of a model by Lexcellent et al. [18] and come to the case when λ_2 is not close to 1 below. Lexcellent et al.'s model for the determination of the yield surface is based on the idea that, in a single crystal, the favorite martensite variant is the one with the largest phase transformation strain along the direction of applied stress, cf. also [30]. The interaction between the grains is neglected.

Assuming $\lambda_1 \leq \lambda_2 = 1 \leq \lambda_3$, we know that a single variant of martensite is compatible with austenite. The compatibility equation (2) then reads $\mathbf{R}_i\mathbf{U}_i - \mathbf{1} = \mathbf{b_i} \otimes \mathbf{m_i}$, which is also called habit plane equation. The values for $\mathbf{R}_i$, $\mathbf{m}_i$ and $\mathbf{b_i}$ can be calculated with the lattice parameter values of the austenite and martensite, which are measured by X-ray. Hence $\mathbf{U}_i$ is obtained.
Moreover, in the framework of the nonlinear theory of martensite, which is used in [18], the transformation strain tensor of a single variant of martensite is

$$\boldsymbol{e}_i^t = \frac{1}{2}(\mathbf{U}_i^2 - \mathbf{1}),$$

which is also called Green-Lagrange strain, see, e.g., [31, Section 2.6].

To obtain the yield curve of a polycrystalline shape-memory alloy which shows interfaces of austenite with single variants of martensite, Lexcellent et al. [18] proceed as follows. Let the polycrystal consist of N grains and suppose that it is isotropic. Moreover, let K denote the driving force for the phase transformation and set $\boldsymbol{\varepsilon}_i^t = \mathbf{R}^T\boldsymbol{e}_i^t\mathbf{R}$, where $\mathbf{R}$ is a rotation from the reference frame to the geometric sample frame. Then there holds

$$\boldsymbol{\sigma} : \boldsymbol{\varepsilon}_i^t = K.$$

For each given $\boldsymbol{\sigma}$ and each grain j, Lexcellent et al. determine the variant $\mathbf{U}_i$ of martensite that gives a maximal K. The latter is denoted by

$$K_j^{\max} := \max_{i=1,\dots,\nu} \boldsymbol{\sigma} : \boldsymbol{\varepsilon}_i^t = \max_{i=1,\dots,\nu} \boldsymbol{\sigma} : \mathbf{R}^T \mathbf{e}_i^t \mathbf{R}, \tag{3}$$

where $\mathbf{R}$ is here understood as a fixed constant rotation which corresponds to grain j. Similarly, the maximal driving force with respect to uniaxial tension $\boldsymbol{\sigma}_{\text{tension}}$ is given by

$$K_{\text{tension},j}^{\max} := \max_{i=1,\dots,\nu} \boldsymbol{\sigma}_{\text{tension}} : \boldsymbol{\varepsilon}_i^t, \tag{4}$$

where, again, the orientation corresponding to grain j is kept fixed. This term is used to normalize the transformation yield stress to 1 for uniaxial tension. Lexcellent et al. [18] then define the transformation yield stress by

$$\boldsymbol{\sigma}^t := \frac{1}{\lambda}\boldsymbol{\sigma} \quad \text{where} \quad \lambda := \frac{\sum_{j=1}^N K_j^{\max}}{\sum_{j=1}^N K_{\text{tension},j}^{\max}}. \tag{5}$$

They simulated this for CuAlBe which has interfaces between austenite and single variants of martensite; the thin line in Figure 3 shows their result. The simulation agrees well with the experimental results. Similar results are obtained for CuZnAl [18].

In the second case, i.e., if λ_2 is not close to 1, the so-called twinning equation

$$\mathbf{R}_{ij}\mathbf{U}_i - \mathbf{U}_j = \mathbf{a} \otimes \mathbf{n} \tag{6}$$

must be solved to obtain compatible pairs (i, j) of variants of martensite. Here, $\mathbf{R}_{ij}$ is a rotation matrix, $\mathbf{n}$ is the normal to the twinning interface and $\mathbf{a}$ is some vector in $\mathbb{R}^3$. If (6) is satisfied, an interface between austenite and these pairs of martensite can occur.
Let the martensite variant $\mathbf{U}_i$ have volume fraction λ and $\mathbf{U}_j$ have volume fraction $1 - \lambda$. Then the compatibility condition (2) reads

$$\mathbf{F} - \mathbf{1} = \mathbf{Q}\big(\lambda \mathbf{R}_{ij}\mathbf{U}_i + (1-\lambda)\mathbf{U}_j\big) - \mathbf{1} = \mathbf{Q}\big(\mathbf{U}_j + \lambda \mathbf{a} \otimes \mathbf{n}\big) - \mathbf{1} = \mathbf{b} \otimes \mathbf{m},$$

where the second equality follows from the twinning equation (6). Again, once the crystallographic parameters are measured, all remaining parameters can be calculated from these equations.
The value of λ as well as the strain tensors $\mathbf{e}_i^t$ and $\mathbf{e}_j^t$ give the strain tensor of the twinned martensite

$$\mathbf{e}_{i,j}^t = \lambda \mathbf{e}_i^t + (1-\lambda)\mathbf{e}_j^t. \tag{7}$$

From this, Lexcellent and Blanc [28] derive formulae for the yield stress in the case of interfaces between austenite and twinned martensite. The obtained formulae are similar to the ones above: replace $\boldsymbol{\varepsilon}_i^t$ in equations (3) and (4) by the strain in the twinned configuration $\boldsymbol{\varepsilon}_{ij}^t = \mathbf{R}^T \mathbf{e}_{ij}^t \mathbf{R}$, cf. (7). The formula for the yield stress is then as in (5).

A numerical simulation of $\boldsymbol{\sigma}^t$ in a CuAlNi polycrystal is shown in Figure 6, taken from [28]. CuAlNi undergoes a cubic to orthorhombic phase transformation, and the CTM predicts

an interface between twinned martensite and austenite. The shape of the predicted CuAlNi curve gives the same properties obtained for CuZnAl and CuAlBe alloys: for instance, the curve is symmetric with respect to the $\sigma_1 = \sigma_2$-axis and it shows an asymmetry between tension and compression. We conclude that the prediction given by the above simulation is qualitatively good, even if no multiaxial loading experiment has been performed on this alloy so far. Such experiments will also allow to decide whether the predicted yield curve fits the data well in all quadrants.
As an aside, we note that the asymmetry between tension and compression on CuAlNi was observed on CuAlNi single crystals with three different orientations by Shield [32].

Finally, we mention that a similar but simpler approach allows the determination of the yield curve in a single crystal material; the single crystal is then treated as one grain of a polycrystal. For instance, Figure 1 shows the simulation of the yield curve of CuZnAl single crystal [33].

6 Model in the framework of energy minimization, crystallography and texture

In this section we discuss a model by Bhattacharya and Schlömerkemper [34]. As in the previous section, the model is based on the CTM. It is assumed that stress-free minimizers of the free energy are also useful to model crystals under applied load. In contrast to the previous section, which uses the geometrically nonlinear theory, this model is in the framework of the geometrically linear theory of martensitic transformations. That is, if $\mathbf{u} \in \mathbb{R}^3$ is the displacement with respect to the austenite (reference configuration), then $\mathbf{e} = \frac{1}{2}(\nabla \mathbf{u} + \nabla \mathbf{u}^T)$ is the so-called linearized strain tensor. For a comparison of the geometrically linear theory with the fully nonlinear theory see [35].
Furthermore, the model of this section uses ideas of Bhattacharya and Kohn's work [14] in homogenization, what we outline below. The approach for polycrystalline alloys is motivated by corresponding formulae for single crystals, which we therefore recall first. Secondly we present the ideas and formulae of the model for polycrystals. At the end of this section and in Section 7 we discuss its results.

Let the energy densities $W_a(\mathbf{e})$ and $W_m(\mathbf{e})$ model the austenite and martensite wells, respectively. Then the stored energy density of a single crystal shape-memory alloy is given as $W(\mathbf{e}) = \min\{W_a(\mathbf{e}), W_m(\mathbf{e})\}$. Moreover, Bhattacharya and Schlömerkemper [34] write the applied load $\boldsymbol{\sigma}$ in terms of a "strength" modulus $\sigma \in \mathbb{R}$ and a matrix $\boldsymbol{\Sigma}_0$ which describes the "direction" of the applied load: $\boldsymbol{\sigma} = \sigma \boldsymbol{\Sigma}_0$. This splitting is motivated by the proportional loading experiments described above; there, "directions" of the applied load $\boldsymbol{\sigma}$ are fixed, and then the "strength" is changed until a phase transformation from austenite to martensite is observed.
The following minimization problem is taken as the starting point to describe dead loading experiments in single crystal shape-memory alloys [36]:

$$\min_{\mathbf{e}} \frac{1}{\mathrm{Vol}(\Omega)} \int_\Omega \big(W(\mathbf{e}) - \sigma \boldsymbol{\Sigma}_0 : \mathbf{e}\big)\, dx,$$

where $\Omega \subset \mathbb{R}^3$ denotes the domain of the crystal in its reference configuration and the minimization is taken over all strains $\mathbf{e}$.
In a single crystal, the integrand is independent of $x \in \Omega$. Therefore it is sufficient to minimize the integrand of the above functional, i.e., to consider $\min_{\mathbf{e}} \big(W(\mathbf{e}) - \sigma\boldsymbol{\Sigma}_0 : \mathbf{e}\big)$. Bhattacharya and Schlömerkemper define the yield stress in single crystals to be the smallest stress σ_Y for which holds

$$\min_{\mathbf{e}} \big(W(\mathbf{e}) - \sigma\boldsymbol{\Sigma}_0 : \mathbf{e}\big) = \begin{cases} \min_{\mathbf{e}} \big(W_a(\mathbf{e}) - \sigma\boldsymbol{\Sigma}_0 : \mathbf{e}\big), & \sigma \leq \sigma_Y \\ \min_{\mathbf{e}} \big(W_m(\mathbf{e}) - \sigma\boldsymbol{\Sigma}_0 : \mathbf{e}\big), & \sigma > \sigma_Y \end{cases} . \tag{8}$$

To obtain explicit formulae, they consider the constrained model (infinitely steep energy densities, $\mathbb{C} \to \infty$), i.e.,

$$W_a(\mathbf{e}) = \begin{cases} 0 & \text{if } \mathbf{e} = 0 \\ \infty & \text{else} \end{cases} \qquad \text{and} \qquad W_m(\mathbf{e}) = \begin{cases} w & \text{if } \mathbf{e} = \mathbf{e}_i^t,\ i = 1, \dots, \nu \\ \infty & \text{else} \end{cases} ,$$

where $\mathbf{e}_i^t$, $i = 1, \dots, \nu$ are the transformation strains of the martensite. In the context of the geometrically linear theory these are defined as $\mathbf{e}_i^t = \mathbf{U}_i - \mathbf{1}$ (Cauchy strain). By (8), the yield stress for a given stress "direction" $\boldsymbol{\Sigma}_0$ is then given by

$$\sigma_Y = \frac{w}{\max_i\ \boldsymbol{\Sigma}_0 : \mathbf{e}_i^t} =: \sigma_{Y_1}, \tag{9}$$

which can be written in terms of the convex hull of the transformation strains

$$\sigma_{Y_1} = w\Big(\max_{\mathbf{e} \in \mathrm{co}\{\mathbf{e}_i^t\}} \boldsymbol{\Sigma}_0 : \mathbf{e} \Big)^{-1}. \tag{10}$$

This motivates why it is useful to work in the framework of the geometrically linear theory here: A result by Bhattacharya [35] allows to relate the convex hull of the transformation strains to the set $\mathcal{S}$ of recoverable strains in a single crystal, i.e., the set of all strains which can be achieved by stress-free mixture of martensite variants below the transformation temperature. This set is given by the minimizers of the quasiconvex hull of W_m. In the full nonlinear theory, quasiconvex envelopes of energies of shape-memory alloys are only known explicitly for a few examples, see e.g., [37] for details about quasiconvex hulls. However, in the context of the geometrically linear theory, the quasiconvex envelope is easier to calculate since Bhattacharya [35] proved: If all transformation strains $\mathbf{e}_i^t$, $i = 1, \dots, \nu$, are pairwise compatible, then $\mathcal{S} = \mathrm{co}\{\mathbf{e}_i^t\}$. Here, two transformation strains $\mathbf{e}_i^t$ and $\mathbf{e}_j^t$ are called compatible if $\mathbf{e}_i^t - \mathbf{e}_j^t = \frac{1}{2}(\mathbf{a} \otimes \mathbf{n} + \mathbf{n} \otimes \mathbf{a})$ for some vectors $\mathbf{a}, \mathbf{n} \in \mathbb{R}^3$. The transformation strains for cubic-to-tetragonal, cubic-to-trigonal and cubic-to-orthorhombic phase transformations have pairwise compatible transformations strains [35]. Note that this does not hold for cubic-to-monoclinic phase transformations, where it is only known that $\mathcal{S}_{\mathrm{mono}} \subset \mathrm{co}\{\mathbf{e}_i\}$.
For later reference in the polycrystalline case, we note that, if the martensitic wells of a phase transformation are pairwise compatible, (10) becomes

$$\sigma_{Y_1} = w\Big(\max_{\mathbf{e} \in \mathcal{S}} \boldsymbol{\Sigma}_0 : \mathbf{e} \Big)^{-1}. \tag{11}$$

The yield stress σ_{Y_1} does not take microstructures of martensite and interfaces between martensite and austenite into account. Bhattacharya and Schlömerkemper therefore give a second definition of the yield stress, σ_{Y_2}, which takes interfaces of austenite with any microstructure of martensite into account. Notice that the strain of undistorted austenite is 0 in the geometrically linear theory. Let the strain of the martensite by $\mathbf{e}$. Then this is compatible with austenite if $\mathbf{e} = \frac{1}{2}(\mathbf{a} \otimes \mathbf{b} + \mathbf{b} \otimes \mathbf{a})$ for some vectors $\mathbf{a}, \mathbf{b} \in \mathbb{R}^3$. Hence

$$\sigma_{Y_2} := w\Big(\max_{\substack{\mathbf{e} \in \mathrm{co}\{\mathbf{e}_i^t\} \\ \mathbf{e} = \frac{1}{2}(\mathbf{a}\otimes\mathbf{b} + \mathbf{b}\otimes\mathbf{a})}} \boldsymbol{\Sigma}_0 : \mathbf{e} \Big)^{-1}. \tag{12}$$

Thirdly, interfaces between austenite and twinned martensite are assumed. That is, $\mathbf{e}$ is given by $\mathbf{e} = \lambda \mathbf{e}_i^t + (1-\lambda)\mathbf{e}_j^t$ for some volume fraction $\lambda \in (0,1)$, and $\mathbf{e}$ is compatible with austenite. Thus

$$\sigma_{Y_3} := w\Big(\max_{\substack{\mathbf{e} = \lambda \mathbf{e}_i^t + (1-\lambda)\mathbf{e}_j^t \\ \mathbf{e} = \frac{1}{2}(\mathbf{a}\otimes\mathbf{b} + \mathbf{b}\otimes\mathbf{a})}} \boldsymbol{\Sigma}_0 : \mathbf{e} \Big)^{-1}. \tag{13}$$

A comparison of the three definitions of transformation yield stresses in single crystals gives

$$\sigma_{Y_1} \leq \sigma_{Y_2} \leq \sigma_{Y_3}, \tag{14}$$

which indicates a dependence of the yield stress on twinning and austenite-martensite interfaces.

In the case of polycrystalline shape-memory alloys, Bhattacharya and Schlömerkemper [34] introduce a texture dependent model. The texture of the polycrystal is described by a piecewise constant rotation-valued function $\mathbf{R} : \Omega \to \mathrm{SO}(3) = \{\mathbf{R} \in M^{3\times 3} : \mathbf{R}^T\mathbf{R} = \mathbf{R}\mathbf{R}^T = \mathbb{1}, \det \mathbf{R} = 1\}$. Now, the energy density of the alloy depends on $x \in \Omega$ and reads

$$W(x, \mathbf{e}) = \min\big\{W_a(\mathbf{R}^T(x)\mathbf{e}\mathbf{R}(x)), W_m(\mathbf{R}^T(x)\mathbf{e}\mathbf{R}(x))\big\},$$

where W_a and W_m are the austenite and martensite energy densities, respectively, from above. Analogously to the single crystal case, the variational problem for the shape-memory alloy under an applied load $\boldsymbol{\sigma} = \sigma\boldsymbol{\Sigma}_0$ is

$$\min_{\mathbf{e}} \frac{1}{\mathrm{Vol}(\Omega)} \int_\Omega \big(W(x, \mathbf{e}) - \sigma\boldsymbol{\Sigma}_0 : \mathbf{e}\big)\, dx. \tag{15}$$

In polycrystals the integrand causes mathematical difficulties due to its x-dependence. Indeed, contrary to the single crystal case, one cannot simply minimize the integrand instead of (15). To avoid this difficulty, upper and lower bounds are considered. We review here only the ones which are based on the notions of the Sachs bound and the Taylor bound, for further definitions of the yield stress see [34].
Firstly, we discuss the Sachs bound on the yield stress. This corresponds to assuming constant stress throughout the crystal. Each grain is then regarded as an independent single

crystal and it is optimized over all grains, i.e., over all rotations $\mathbf{R}$ related to the polycrystal. With σ_{Y_1} in (9) the Sachs bound on the yield stress then reads

$$\sigma_{Y_S} = \min_{\mathbf{R}} w\Big(\max_{i=1,\dots,\nu} \ \mathbf{\Sigma}_0 : \mathbf{R}^T \mathbf{e}_i^t \mathbf{R} \Big)^{-1} = w\Big(\max_{i=1,\dots,\nu;\, \mathbf{R}} \ \mathbf{\Sigma}_0 : \mathbf{R}^T \mathbf{e}_i^t \mathbf{R} \Big)^{-1}. \tag{16}$$

In Section 7 we compare this bound on the yield stress with the yield stress defined in (5). A plot of the Sachs bound on the yield stress is given in [38] for CuAlNi (cubic-to-orthorhombic phase transformation) with isotropic and uniaxial texture, respectively, cf. the left plot in Figure 7. Here, isotropic refers to a polycrystal with no texture, and uniaxial (transversally isotropic) texture means that the orientations of the grains can be described by all rotations about one prescribed axis, which is assumed to be orthogonal to the eigenstress space (σ_1, σ_2). Both yield curves show the expected symmetry with respect to the $\sigma_1 = \sigma_2$-axis. They also show an asymmetry in tension and compression; this is however contrary to the expected one. As the Sachs bound is a lower bound on the real yield stress (see below), we guess that the Sachs bound underestimates the values in compression too much. Furthermore, it seems to be interesting to study analogous definitions of the Sachs bound based on (12) or (13) instead of (9), which thus would include effects of microstructure or austenite-martensite interfaces. However, in the end, further interpretations depend on results of multiaxial proportional loading experiments in CuAlNi, which are a task for future research.

The Taylor bound on the yield stress is based on the assumption of constant strain throughout the crystal. For this set

$$\mathcal{T} := \bigcap_{x \in \Omega} \mathcal{S}(x) = \{ \mathbf{e} \ : \ \mathbf{R}^T(x) \mathbf{e} \mathbf{R}(x) \in \mathcal{S} \ \text{ for each } \ x \in \Omega \},$$

and confer [14] for details. The Taylor bound $\mathcal{T}$ was studied in a series of papers by Bhattacharya and Kohn [39, 14] and Shu and Bhattacharya [40] to understand when and whether a polycrystalline material is a good shape-memory alloy. Using the framework of geometrically linear elasticity, they showed that the underlying phase transformation as well as the texture of the polycrystal have an influence on the size of $\mathcal{T}$. Explicit formulae for $\mathcal{T}$ are given for several phase transformations and textures.

Motivated by (11) in the case of single crystals, Bhattacharya and Schlömerkemper [34] set

$$\sigma_{Y_T} := w\Big(\max_{\mathbf{e} \in \mathcal{T}} \mathbf{\Sigma}_0 : \mathbf{e} \Big)^{-1} \tag{17}$$

to estimate the yield stress of a polycrystalline shape-memory alloy by using the Taylor bound. The bound σ_{Y_T} is calculated explicitly in [34] for cubic-to-orthorhombic phase transformations in biaxial loading experiments (with w set equal to 1), cf. Figure 8, where the two cases of isotropic and uniaxial texture are considered. The two different curves clearly show the influence of texture on the Taylor bound of the transformation yield stress. The yield stress for the isotropic material is larger than the one for the uniaxial material, which also becomes apparent in the formula for the Taylor set $\mathcal{T}$ and hence in the definition of σ_{Y_T} in (17). Moreover, the yield curves show the expected asymmetry in tension and compression as well as a mirror symmetry with respect to the $\sigma_1 = \sigma_2$-axis. Again, a quantitative

comparison of the texture-dependent Taylor yield curves remains an open problem until corresponding experimental results are available. (As an aside, note that the plots of the Taylor bound are not normalized by the yield stress in pure tension as is done is some of the other Figures.)

The real yield stress is expected to lie in between the Sachs and the Taylor bounds, i.e., $\sigma_{Y_S} \leq \sigma_Y \leq \sigma_{Y_T}$ [34]. See also the right plot in Figure 7 and confer [38] for a more detailed comparison of the Sachs and the Taylor bound.

7 Comparative discussion

The aim of this section is to contrast and compare the different models presented and to mention open problems for future work.

Firstly, we note common features of the models. All models which we presented in this article (apart from the Sachs bound) give yield curves which show the widely experimentally observed asymmetry in tension and compression. Moreover, all yield curves—apart from the right figure in Figure 5 (textured material)—show a mirror symmetry with respect to the $\sigma_1 = \sigma_2$-axis, which is also observed experimentally.
As summarized in Section 2, multiaxial proportional loading experiments have been performed on polycrystals as well as on a single crystal. We note that all presented models (can) consider the transformation yield surface in single crystals as well as in polycrystals.

Secondly, we point out differences of the models presented and summarize the different assumptions made. This regards among others the kind of solid-solid phase transformation, assumptions of constant stress or strain, interaction of grains, the influence of twin boundaries and the influence of texture. All models make some simplifying assumptions in order to estimate the real yield stress. The question is which model describes the observed yield surfaces best; this has been our motivation for contrasting the models in this article. However, as it turns out, the search for an answer poses further open problems which have to be tackled before we can give a final, satisfying answer. We outline these problems below and hope to stimulate research on these topics.

The two models based on the crystallographic theory of martensite reflect the different kind of phase transformations, explicitly, cf. formuluae (3)–(5), (10)–(13), and (16) and (17). Hence these models state a dependence of the yield surface on the kind of phase transformation. The phenomenological model in Section 3 does not depend explicitly on the kind of phase transformation; the yield curve was fitted for CuZnAl and CuAlBe, which show a cubic-to-monoclinic transformation. The self-consistent scheme presented in Section 4 takes the number of habit plane variants as well as the phase transformation strains into account. The plot in Figure 5 is also for a cubic-to-monoclinic alloy.
Multiaxial loading experiments have only been performed for cubic-to-monoclinic phase transformations in polycrystalline shape-memory alloys (CuZnAl, CuAlBe, NiTi, cf. Section 2 for references) so far. Measurements for other kind of solid-solid phase transformations in polycrystalline shape-memory alloys are an open task. It would be interesting to see

whether the predicted dependence of the yield surface on the kind of phase transformation can be verified experimentally.

The influence of twin boundaries and austenite-martensite interfaces is discussed in the context of the models discussed in Sections 5 and 6. In the model based on energy minimization this is apparent in (14) in connection with (10)–(13). The (theoretical) yield stress becomes larger the more constraints on the transformation strain tensors are considered. Indeed, if there are more constraints imposed, the maximum of $\mathbf{\Sigma}_0 : \mathbf{e}$ can become smaller. Thus the inverse of this maximum, which is related to the yield stress, can become larger. Hence these models indicate a dependence of the yield surface on austenite-martensite interfaces and twin boundaries. This is also apparent in a study by Lexcellent and Blanc [28] for the determination of the yield curve for NiTi using the micro-macro model (Section 5). They did one calculation under the assumption of having single variants of martensite and another calculation assuming twinned martensite, which gives two different yield curves. Interestingly, the former curve fits experimental results better [28].
In the self-consistent model, the influence of habit planes is taken into account phenomenologically: the interaction matrix H^{ij} favors compatible microstructures over non-compatible ones [23].

It is known that loading conditions are not uniform in polycrystalline materials. This is taken into account in the self-consistent model [26] by some intergranular stress field, but is neglected in the other models. These models assume that grain boundary interactions are negligible small. For the Sachs bound and in the micro-macro model, constant stress throughout the sample is assumed. Note that in this sense, also the micro-macro model gives a kind of a Sachs bound. However, for definiteness we only call the Sachs bound in Section 6 Sachs bound in this article.
As announced earlier, we next discuss the yield stress in the 'micro-macro' model (5) and the Sachs bound (16) comparatively, cf. also Figures 3 and 6, and Figure 7. The most striking difference between the estimates of the yield curves obtained by the micro-macro model and the model based on energy minimization, respectively, is that there are polygons in the latter and smooth curves in the former. Otherwise, the models give consistent results.
From a modeling point of view, the main differences between the two models are that the micro-macro model is based on the fully nonlinear theory of martensite and takes twinning and austenite-martensite interfaces into account, while the Sachs bound as defined in (16) neglects twinning and austenite-martensite interfaces and is phrased in the geometrically linear theory of martensite. Here we want to point out a further aspect: Recall that the "strength" of the yield stress in (5) is given by

$$\frac{1}{\lambda}\sigma = \frac{\sum_{j=1}^{N} K^{\max}_{\text{tension},j}}{\sum_{j=1}^{N} K^{\max}_{j}}\sigma = \frac{\frac{1}{N}\sum_{j=1}^{N} K^{\max}_{\text{tension},j}}{\frac{1}{N}\sum_{j=1}^{N} K^{\max}_{j}}\sigma,$$

where we write $\boldsymbol{\sigma} = \sigma\mathbf{\Sigma}_0$ as before. For a comparison with the Sachs bound (16) we set $w_{\text{tension}} = \frac{1}{N}\sum_{j=1}^{N} K^{\max}_{\text{tension},j}$; the normalization factor w_{tension} depends on the orientation of the grains and their number. By (3) we then obtain

$$\frac{1}{\lambda}\sigma = \frac{w_{\text{tension}}}{\frac{1}{N}\sum_{j=1}^{N} \max_{i=1,\dots,\nu} \ \mathbf{\Sigma}_0 : \mathbf{R}^T\mathbf{e}_i^t\mathbf{R}}. \tag{18}$$

In the model based on energy minimization, the Sachs bound $(16)_2$ on the "strength" of the yield stress reads

$$\frac{w}{\max_{i=1,\dots,\nu;\,\mathbf{R}}\ \boldsymbol{\Sigma}_0 : \mathbf{R}^T\mathbf{e}_i^t\mathbf{R}}. \tag{19}$$

That is, instead of averaging over all grains that grain/rotation is picked which maximizes $\max_{i=1,\dots,\nu} \boldsymbol{\Sigma}_0 : \mathbf{R}^T\mathbf{e}_i\mathbf{R}$, which makes the occurrence of polygons likely. The denominator of (18) shows an arithmetic average of the contributions of all grains. This gives a smooth curve for large N. It is interesting to note that the yield curve of single crystal CuZnAl obtained on the basis of the micro-macro model also has flat parts and corners, cf. Figure 1. Yield curves with corners are also obtained for the Taylor bound, cf. Figure 8. Rudimentally, the yield curves for some textures studied in [20], cf. Figure 5, can be considered as having a corner-like shape. However, whether this can also be observed in experiments remains open.

Next we discuss the influence of texture, which was studied in the models presented in Sections 4 and 6. For related work in one-dimensional experiments cf. [9]. Recall that the Taylor set $\mathcal{T}$ and hence the Taylor bound on the yield stress depend on the underlying texture, cf. (17). The Taylor bound on the yield curve obtained for uniaxial texture shows relatively large values for the yield stress in the second and fourth quadrant, whereas the Sachs bound gives relatively small values in these quadrants, cf. Figures 7 and 8. This is not what we would expect, in particular in comparison with the numerical yield curves in Figure 5 and similar simulated ones which are obtained for drawn texture in [20], see also the experimental results in [32]. On the other hand, the Sachs as well as the Taylor bound capture typical expected behavior of the yield curves. It will be interesting to see whether the experiments being in progress on rolled and drawn CuAlBe samples, cf. Section 4, verify a dependence of the yield curve on the initial texture and whether they show curves with corners.

Finally we mention an open mathematical problem related to the influence of the kind of phase transformation. Note that $\mathcal{T}$ can be calculated explicitly for all solid-solid phase transformations and textures; only the cubic-to-monoclinic transformations causes difficulties, cf. the discussion before (11). Since multiaxial loading experiments and numerical simulations have only been performed in alloys with a cubic-to-monoclinic phase transformation so far, this case would be in particular interesting. That is, there is some need for a better mathematical understanding of the Taylor set for cubic-to-monoclinic transformations.

8 Conclusion

We have reviewed several experimental, theoretical and mathematical works which determine the yield surface of shape-memory alloys obtained in multiaxial proportional loading experiments. The models are phrased in different theoretical contexts and make different simplifying assumptions, which makes it interesting to compare them. For instance, there are phenomenological models in the framework of thermodynamics and models based on the crystallographic theory of martensite. Some models take the kind of phase transformation

into account and some also study the influence of texture. Despite these differences, the qualitative results of the models reviewed in this article are mainly first of all good as they show the experimentally observed asymmetry in tension and compression as well as the symmetry with respect to the $\sigma_1 = \sigma_2$-axis.
In order to say whether the models are also good from a quantitative point of view, more experimental work needs to be done. Experimental determination of the yield surface would in particular be interesting with respect to texture dependence and dependence on the inherent phase transformation.

Appendix: Summary of notation

$\boldsymbol{\sigma}$	applied external stress tensor
$\mathrm{dev}(\boldsymbol{\sigma})$	deviatoric stress tensor
$\boldsymbol{\varepsilon}$	total strain tensor
$\boldsymbol{\epsilon}_i^t$	transformation strain tensor corresponding to the ith habit plane (in the theory of Wechsler et al. [24])
$\boldsymbol{e}_i^t$	phase transformation strain tensor of variant i, $i = 1, \ldots, \nu$ (Green-Lagrange strain)
$\boldsymbol{\varepsilon}_i^t$	phase transformation strain tensor (Green-Lagrange) of ith variant in the geometric sample frame, $i = 1, \ldots, \nu$
$\mathbf{e}_i^t$	phase transformation strain tensor (Cauchy) in the geometrically linear setting, $i = 1, \ldots, \nu$
z_n	volume fraction of nth variant of martensite
$z = \sum_n z_n$	global volume fraction of martensite, internal variable
$1 - z$	global volume fraction of austenite
Π^f	thermodynamic force associated to global fraction of martensite z
Π_n^f	thermodynamic force associated to fraction of martensite variant z_n
$\mathbf{S}$	stiffness matrix
H^{nm}	interaction matrix between martensite variants.
K	driving force for phase transformation

Acknowledgement: This work was partially supported through TMR-grant FMRX-CT 98-0229 ("Phase transitions in crystalline solids"), while AS was working at the Mathematical Institute in Oxford in the group of John Ball, whom both authors would like to thank for stimulating discussions at the beginning of this project. A visit of CL at the Institute of Analysis, Dynamics and Modelling at the University of Stuttgart, with which AS was affiliated at that time, was supported by the DFG Priority Programm 1095.

References

[1] Bhattacharya K. Microstructure of martensite, Oxford series of materials modelling, Oxford University Press, 2003

[2] James RD, Hane KF. Martensitic transformations and shape-memory materials. Acta mater 2000;48:197–222

[3] Gall K, Sehitoglu H, Maier HI. Asymmetric stress-strain response in shape memory alloys. In: Plasticity 97. Juneau (USA) 1997, pp. 153–4

[4] Orgéas L, Favier D. Stress-induced martensitic transformation of a NiTi alloy in isothermal shear, tension and compression. Acta mater 1998;46:5579–91

[5] Raniecki B, Tanaka K, Ziolkowski A. Testing and modelling at complex stress state. Selected results of Polish-Japanese research cooperation. Mat Sci Res Int 2001;2:327–34

[6] Vacher P, Lexcellent C. Study of Pseudoelastic Behavior of Polycrystalline Shape Memory Alloys by Resistivity Measurements and Acoustic Emission. In: Proceedings of ICM VI, 1991, pp. 231–6

[7] Sittner P, Liu Y, Novak V. On the origin of Lüders-like deformation of NiTi shape memory alloys. J Mech Phys Solids 2005;53:1719–46

[8] Novák V, Šittner P. Micromechanics modelling of NiTi polycrystalline aggregates transforming under tension and compression stress. Mat Sci Eng A 2004;378:490–8

[9] Thamburaya P, Anand L. Polycrystalline shape-memory materials: effect of crystallographic texture. J Mech Phys Solids 2001; 49:709–37

[10] Hackl K, Schmidt-Baldassari M, Zhang W. A micromechanical model for polycrystalline shape-memory alloys. Mat Sci Eng A 2004; 378:503–6

[11] Bouvet C, Calloch S, Lexcellent C. Mechanical Behavior of a Cu-Al-Be Shape Memory Alloy Under Multiaxial Proportional and Nonproportional Loadings. J Eng Mat and Techn 2002;124:112–24

[12] Ball JM, James RD. Fine phase mixtures as minimizers of energy. Arch Rational Mech Anal 1987;100:13–52

[13] Ball JM, James RD. Proposed experimental tests of a theory of fine microstructure and the two-well problem. Phil Trans Roy Soc Lond A 1992;338:389–450

[14] Bhattacharya K, Kohn RV. Elastic Energy Minimization and the Recoverable Strains of Polycrystalline Shape-Memory Materials. Arch Rational Mech Anal 1997;139:99–180

[15] Lim TJ, McDowell DL. Mechanical behavior of Ni-Ti shape memory alloys under axial-torsional proportional and nonproportional loading. J Eng Mat and Techn 1999;121:9–18

[16] Gall K, Sehitoglu H, Maier HI, Jacobus K. Stress-induced Martensitic Phase Transformations in Polycrystalline CuZnAl Shape Memory Alloys under Different Stress States. Met Mat Trans A 1998;29A:765–73

[17] Vivet A, Lexcellent C. CuZnAl single crystals pseudoelastic behaviour under biaxial tensile loading: observation and analysis. J Phys IV 2001;11:205–12

[18] Lexcellent C, Vivet A, Bouvet C, Calloch S, Blanc P. Experimental and numerical determinations of the initial surface of phase transformation under biaxial loading in some polycrystalline shape-memory alloys. J Mech Phys Solids 2002;50:2717–35

[19] Bouvet C, Calloch S, Lexcellent, C. A phenomenological model for pseudoelasticity of shape memory alloys under multiaxial proportional and nonproportional loadings. Eur J of Mech A Solids 2004;23:37–61

[20] Aleong D, Dumon C, Arbab Chirani S, Patoor E, McDowell D. Transformation Surfaces of a Textured Pseudoelastic Polycrystalline Cu-Zn-Al Shape Memory Alloy. J of Int Mat Syst and Struct 2002;13:783–93

[21] Arbab Chirani S, Patoor E. Influence of the crystallographic texture on transformation surfaces in shape memory alloys. In: 3rd Japan-France Seminar on Intelligent Materials and Structures. Tokai, 2000, pp. 188–92

[22] Arbab Chirani S, Aleong D, Dumont C, McDowell D, Patoor E. Superelastic behavior modeling in shape memory alloys. J Phys IV France 2003;112:205–8

[23] Siredey N, Patoor E, Berveiller M, Eberhardt A. Constitutive equations for polycrystalline thermoelastic shape memory alloys. Part I. Intragranular interactions and behaviour of the grain. Int J of Solid and Struct 1999;36:4289–315

[24] Wechsler MS, Liebermann DS, Read TA. On the theory of the formation of martensite. Trans AIME J Metals 1953;197:1503–15

[25] Taillard K, Blanc P, Calloch S, Lexcellent C. Phase transformation yield surface of anisotropic shape memory alloys. Proceedings of ICOMAT 05, to appear in Mat Sci Eng A

[26] Entemeyer D, Patoor E, Eberhardt A, Berveiller M. Strain rate sensitivity in superelasticity. Int J of Plasticity 2000;16:1269–88

[27] Hane KF. Bulk and thin film microstructures in untwinned martensites. J Mech Phys Solids 1999;47:1917–39

[28] Lexcellent C, Blanc P. Phase transformation yield surface determination for some shape memory alloys. Acta Mater 2004;52:2317–24

[29] Hane KF and Shield TW. Microstructure in the cubic to monoclinic transition in Titanium-Nickel shape memory alloys. Acta mater 1999;47:2603–17

[30] Huang W. “Yield” surface of shape memory alloys and their applications. Acta mater 1999;47:2769–76

[31] Holzapfel GA. Nonlinear Solid Mechanics. John Wiley & Sons Ltd, Chichester, 2000

[32] Shield TW. Orientation dependence of the pseudoelastic behavior of single crystals of Cu–Al–Ni in tension. J Mech Phys Solids 1995;43:869–895

[33] Lexcellent C, Vivet A, Bouvet C, Blanc P, Satto C, Schryvers D. From the lattice measurements of the austenite and the martensite cells to the macroscopic mechanical behavior of shape memory alloys. J Phys IV France 2001;11:317–24

[34] Bhattacharya K, Schlömerkemper A. Transformation yield surface of shape-memory alloys. J Phys IV France 2004;115:155–62

[35] Bhattacharya K. Comparison of the geometrically nonlinear and linear theories of martensitic transformation. Continuum Mech Thermodyn 1993;5:205–42

[36] James RD. Displacive phase transformations in solids. J Mech Phys Solids 1996;34:359–94

[37] Müller S. Variational models for microstructure and phase transitions. In: Hildebrandt S, Struwe M, editiors. Calculus of variations and geometric evolution problems. Lecture Notes in Math 1999;1713,85–210, Springer-Verlag, Berlin

[38] Schlömerkemper A. On a Sachs bound for stress-induced phase transformations in polycrystalline shape memory alloys. Submitted to PAMM Proc Appl Math Mech 2006

[39] Bhattacharya K, Kohn RV. Symmetry, texture and the recoverable strain of shape-memory polycrystals. Acta mater 1996;44:529–42

[40] Shu YC, Bhattacharya K. The influence of texture on the shape-memory effect in polycrystals. Acta mater 1998;46:5457–73

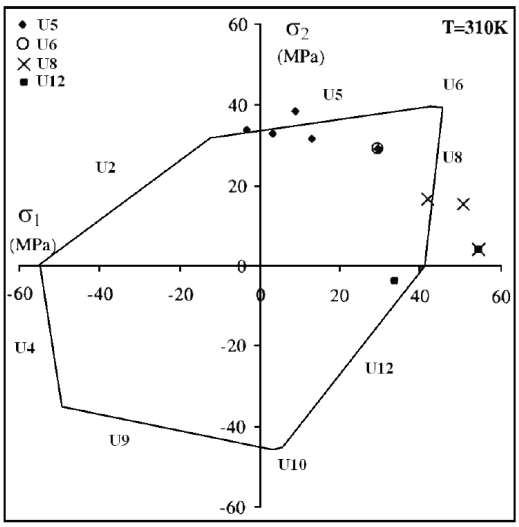

Figure 1: Experimental and numerical results for the yield curve of a CuZnAl single crystal [17]. The numerical result is based on the model described in Section 5. Here, U_i, $i = 1, \ldots, 12$, represents the stretch matrix of the ith variant of martensite.

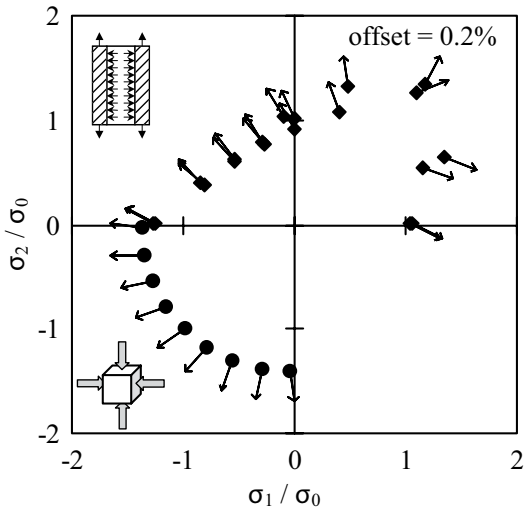

Figure 2: Experimental points of phase transformation initiation for bicompression and tension(compression)-internal pressure tests for CuAlBe polycrystal [18], see also [11]. The normalization factor σ_0 equals the yield stress in pure tension.

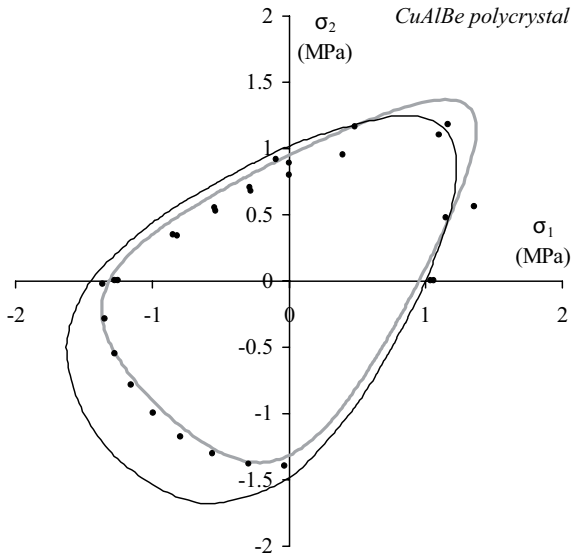

Figure 3: Yield surface of CuAlBe polycrystal, taken from [18]. Note that σ_1 and σ_2 denote here the normalized stress values, i.e., those divided by the value of the yield stress in pure tension. Points = experimental points, thick line = phenomenological simulation as described in Section 3, thin line = micro-macro simulation as described in Section 5.

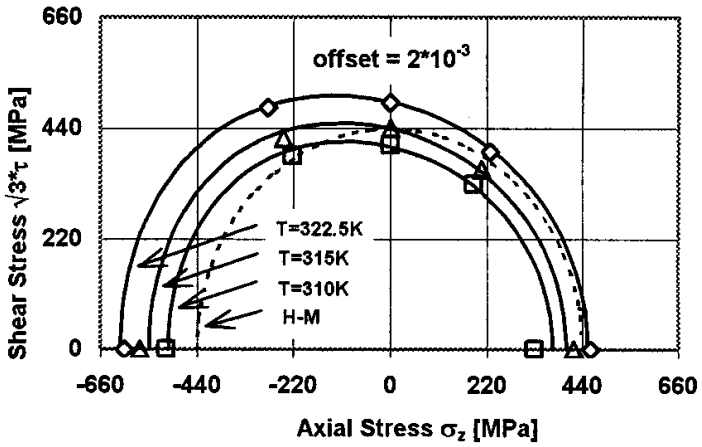

Figure 4: Phenomenological simulation of yield surfaces of NiTi polycrystal for different temperatures [5], cf. Section 3. The dotted line is based on a Huber-Von Mises modeling.

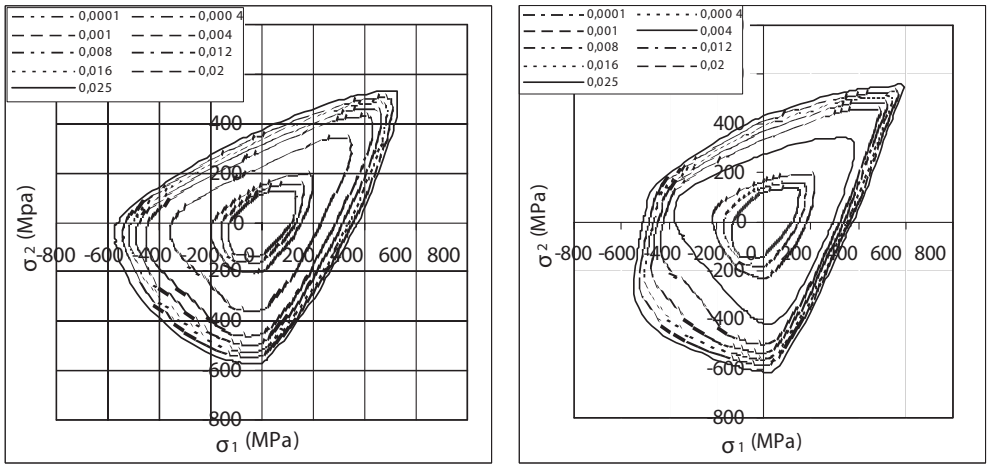

Figure 5: Surfaces of constant strain in CuZnAl for an isotropic crystal (left) and a material with rolled texture (right) [20]. Based on the model described in Section 4.

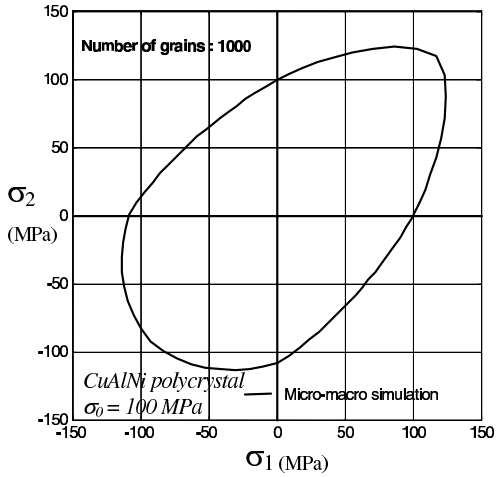

Figure 6: Numerical Simulation of $\boldsymbol{\sigma}^t$ for a CuAlNi polycrystal [28]. Based on the model described in Section 5 (cubic-to-orthorhombic transformation with interface between austenite and twinned martensite).

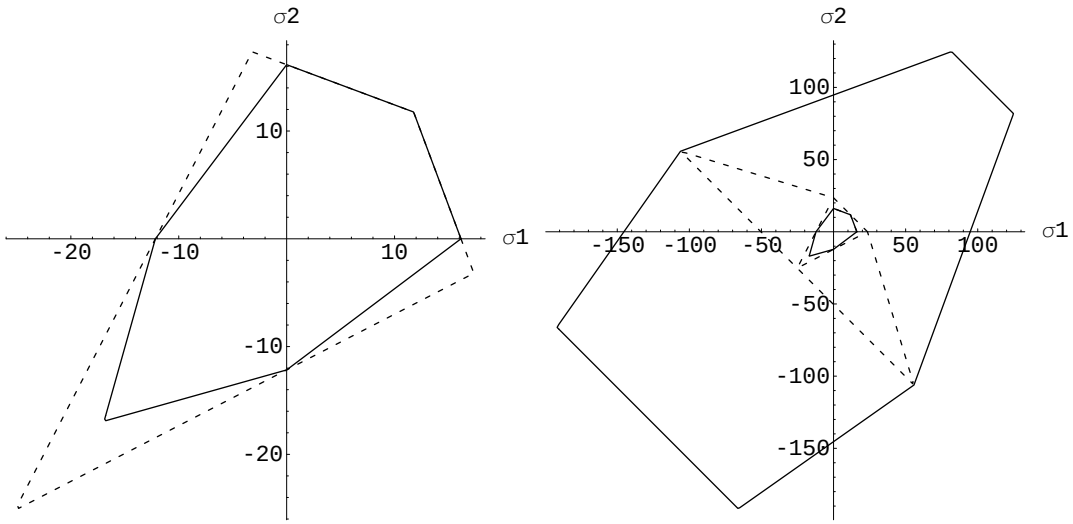

Figure 7: Left: Plot of the Sachs bound σ_{Y_S} on the yield stress for a cubic-to-orthorhombic material (CuAlNi), which is isotropic (—) and has uniaxial (- - -) texture, respectively, [38]. Based on the model described in Section 6. Right: Comparison of the Sachs (inner) and Taylor (outer) yield curves for CuAlNi with isotropic (—) and uniaxial (- - -) texture, respectively.

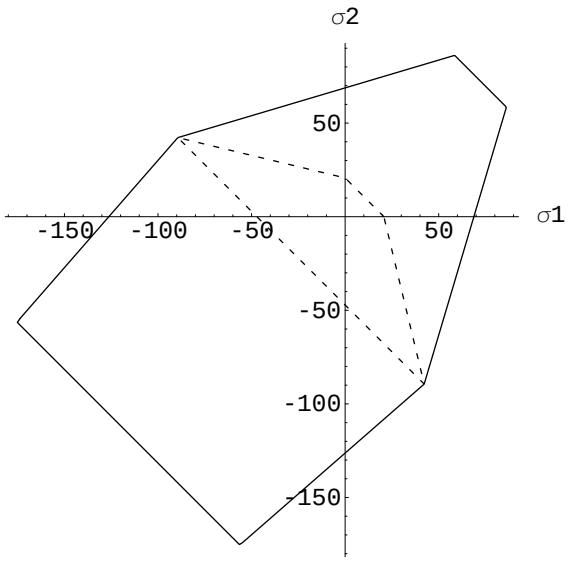

Figure 8: Plot of the Taylor bound σ_{Y_T} on the yield stress for a cubic-to-orthorhombic material, which is isotropic (—) and has uniaxial (- - -) texture, respectively, [34]. Based on the model described in Section 6.